*nanomaterials*

MDPI

*Article*

# 3D Modeling of Silver Doped $ZrO_2$ Coupled Graphene-Based Mesoporous Silica Quaternary Nanocomposite for a Nonenzymatic Glucose Sensing Effects

**Kamrun Nahar Fatema [1], Chang-Sung Lim [1], Yin Liu [2], Kwang-Youn Cho [3], Chong-Hun Jung [4] and Won-Chun Oh [1,2,*]**

[1] Department of Advanced Materials Science & Engineering, Hanseo University, Seosan-si 356-706, Korea; kamrunnahar270@gmail.com (K.N.F.); cslim@hanseo.ac.kr (C.-S.L.)
[2] Anhui International Joint Research Center for Nano Carbon-Based Materials and Environmental Health, College of Materials Science and Engineering, Anhui University of Science & Technology, Huainan 232001, China; yinliu@aust.edu.cn
[3] Korea Institutes of Ceramic Engineering and Technology, Soho-ro, Jinju-si 52851, Korea; kycho@kicet.re.kr
[4] Decommissioning Technology Research Division, Korea Atomic Energy Research Institute, Yuseong, Daejeon 305-600, Korea; nchjung@kaeri.re.kr
* Correspondence: wc_oh@hanseo.ac.kr; Tel.: +82-41-660-1337; Fax: +82-41-688-3352

**Abstract:** We described the novel nanocomposite of silver doped $ZrO_2$ combined graphene-based mesoporous silica ($ZrO_2$-Ag-G-$SiO_2$,) in bases of low-cost and self-assembly strategy. Synthesized $ZrO_2$-Ag-G-$SiO_2$ were characterized through X-ray diffraction (XRD), scanning electron microscopy (SEM), energy-dispersive X-ray spectrometry (EDX), transmission electron microscopy (TEM), high-resolution transmission electron microscopy (HRTEM), Raman spectroscopy, Nitrogen adsorption-desorption isotherms, X-ray photoelectron spectroscopy (XPS), and Diffuse Reflectance Spectroscopy (DRS). The $ZrO_2$-Ag-G-$SiO_2$ as an enzyme-free glucose sensor active material toward coordinate electro-oxidation of glucose was considered through cyclic voltammetry in significant electrolytes, such as phosphate buffer (PBS) at pH 7.4 and commercial urine. Utilizing $ZrO_2$-Ag-G-$SiO_2$, glucose detecting may well be finished with effective electrocatalytic performance toward organically important concentrations with the current reaction of $9.0 \times 10^{-3}$ $mAcm^{-2}$ and 0.05 mmol/L at the lowest potential of +0.2 V, thus fulfilling the elemental prerequisites for glucose detecting within the urine. Likewise, the $ZrO_2$-Ag-G-$SiO_2$ electrode can be worked for glucose detecting within the interferometer substances (e.g., ascorbic corrosive, lactose, fructose, and starch) in urine at proper pH conditions. Our results highlight the potential usages for qualitative and quantitative electrochemical investigation of glucose through the $ZrO_2$-Ag-G-$SiO_2$ sensor for glucose detecting within the urine concentration.

**Keywords:** glucose sensor; electrocatalytic performance; functional stability; interfering agents; urine

check for updates

**Citation:** Fatema, K.N.; Lim, C.-S.; Liu, Y.; Cho, K.-Y.; Jung, C.-H.; Oh, W.-C. 3D Modeling of Silver Doped $ZrO_2$ Coupled Graphene-Based Mesoporous Silica Quaternary Nanocomposite for a Nonenzymatic Glucose Sensing Effects. *Nanomaterials* **2022**, *12*, 193. https://doi.org/10.3390/nano12020193

Academic Editor: Camelia Bala

Received: 7 December 2021
Accepted: 4 January 2022
Published: 7 January 2022

**Publisher's Note:** MDPI stays neutral with regard to jurisdictional claims in published maps and institutional affiliations.



## 1. Introduction

Biosensors are developed for giving symptomatic data for the patient's prosperity status. Electrochemistry, fluorescence, colorimetry, photoelectrochemistry, and chemical luminescence, have been received for glucose sensing [1,2]. Among them, the electrochemical detecting method has gotten high attention due to its high affectability, promising reaction time [3–5]. Glucose oxidation on the sensor is dependable for the chemisorption of the hydroxyl group onto the metal oxide and shaping the bond among the d-electron of metal and glucose atoms. The oxidation state of glucose particles is affected by the metal surface as well as metal-glucose interaction, glucose-metal bond quality, and desorption of glucose particles. By considering an imitating method of the enzyme-like component, a few metals and metal oxides like Au, Pt, Cu, Ni, Mn, Co, and Fe [6–21] have been studied. Limitation of detection (LOD) for the analyte, the typical nanomaterials considered [22]. Graphene

has gotten around the world consideration for the improvement of biosensors because graphene-based biosensors have high electron transfer rates, high charge-carrier mobility, and are extremely significant for biomarkers owing to their extraordinary electrochemical (amperometric, voltammetry, impedimetric) response [23,24]. In addition, graphene shows a thickness of the edge-plane-like structure, giving numerous dynamic destinations for electron transfer to chemical and biological species [23]. Graphene containing zirconium oxide ($ZrO_2$) offers a way to upgrade their application by allowing flexible and ideal electrochemical properties, extraordinary potential applications within the broad fields of sensing [25–30]. The affectability and conductivity of graphene may be advance upgraded by enhancing Ag NPs owing to their high electron transfer for modifiers in biosensors [31,32]. Biocompatibility, nontoxicity, high conductivity, chemical and steadiness of $SiO_2$ make to idealize for utilization for adsorption, biosensors [33,34]. With these points, we developed the $ZrO_2$-Ag-G-$SiO_2$ which was effectively synthesized by the self-assembly method. $ZrO_2$, G, and $SiO_2$ have octahedral coordination, Ag occupies on the $ZrO_2$-G-$SiO_2$ displays giving dynamic response for possible charge transfer to electrolyte [35–37].

In this consideration, $ZrO_2$-Ag-G-$SiO_2$ nanocomposite was developed main active material for glucose sensing. $ZrO_2$-Ag-G-$SiO_2$ was effectively synthesized by utilizing a basic, low-cost, self-assembly method, and was inspected for nonenzymatic glucose oxidation for the quick response. It shows especially high effectiveness for glucose oxidation counting a greatly low working potential of as it were 0.2 V vs Ag/AgCl. In general, $ZrO_2$-Ag-G-$SiO_2$ affirmed a significant response without any electron facilitator, provoking a novel way for glucose sensing within the urine. The electrochemical sensing behavior of the $ZrO_2$-Ag-G-$SiO_2$ sensor towards glucose sensing was examined utilizing amperometric techniques.

## 2. Experimental

### *2.1. Materials*

All chemicals used analytical grade without further modification. Graphite powder (99%), zirconium (IV) isopropoxide (70 wt% in 1-Propanol), Pluronic F127 were purchased from Sigma Aldrich (Seoul, Korea). Ethylene Glycol, $AgNO_3$, HCl, Phosphate Buffer, NaOH, KOH, Ethylene Glycol were purchased from Dae-Jung Chemical Korea (Busan, Korea). Deionized water (18.2 $M\Omega cm^{-1}$) was a self-made product.

### *2.2. Synthesis of $ZrO_2$*

6.5 g of Pluronic F127 was mixed up in 50 mL of ethanol and zirconium (IV) isopropoxide solution was included in 50 mL of ethanol and ethylene glycol separately with vigorous mixing and added together at 314 K with 50 mL of $H_2O$. Hydrochloric acid was included to alter the pH 2.4 and kept at 314 K for 1 h and 354 K in a closed container for 24 h after that dried at 374 K and calcined at 674 K for 5 h.

### *2.3. Synthesis of Silver Doped $ZrO_2$ ($ZrO_2$-Ag)*

3.5 g of $AgNO_3$ was in 50 mL of deionized water. Then $ZrO_2$ was poured dropwise to solution blended till the gel came out. The gel was dried at 374 K for 3·1⁄2 h, calcined at 674 K, and after that ground to get the $ZrO_2$-Ag nanoparticles.

### *2.4. Synthesis of $ZrO_2$-Ag-G*

0.33 g of graphite oxide (GO) was scattered into 300 mL of water and ultra-sonicated for 40 min. Sonicated graphene oxide exchanged poured into $ZrO_2$-Ag solution and 50 mL of 1 M sodium hydroxide included into the sonicated mixture dropwise for expected pH and blended for 3 h at 374 K. The color turned into coffee color, demonstrates the effective combination of G with Ag combined $ZrO_2$ arrangement E.

### 2.5. Synthesis of $ZrO_2$-Ag-G-$SiO_2$

For the synthesis of final nanocomposites, 1.1 g of triblock copolymer Pluronic F-127 was included to 100 mL of deionized water and 61 mL of 2 M HCl at 313 K. 4 mL of tetraethyl orthosilicate (TEOS) was included and blended at 314 K for 12·1⁄2 h and heated to 374 K for 20 h after that washed with water and ethanol and dried at 338 K overnight and the copolymer was calcination at 824 K for 3·1⁄2 h. The solution $ZrO_2$-Ag-G was drop-by-drop included on 0.3 g of the silica powder and this mixture was blended with 374 K for 24 h and ultrasonicated for $1_{1/2}$ h and get the powder, washed with 1.5 mL of methanol, and dried at 338 K overnight. Calcined at 974 K at 283 K/min and held at 974 K for 5 h. Dark color items were found.

### 2.6. Preparation of $ZrO_2$-Ag-G-$SiO_2$ Electrode

The zrO2-Ag-G-SiO2 coated film was prepared using a routine doctor-blade method [38]. For the altered doctor-blade method, we controlled the thickness of $ZrO_2$-Ag, $ZrO_2$-Ag-GO, $ZrO_2$-Ag-GO-$SiO_2$. To begin with, synthesized fabric powder (1.1 g) was mixed with Ethylcellulose and acetone (1.5 mL) in a mortar for 15 min. After that, the prepared glues were coated on FTO glass to create a film, after being dried within the open state for 35 min. One drop greasing up oil was put onto the film surface and stabilized beneath 374 K in the dry oven for 25 min to decrease breaks.

### 2.7. Characterization of the Materials

The phase structure and purity of as-synthesized products were examined by X-ray diffraction (XRD, Rigaku, Chiba, Japan) with Cu-K$\alpha$ radiation ($\lambda$ = 1.5406 Å) at 40 kV, 30 mA over 2$\theta$ range of 20–70. Morphologies were studied utilizing scanning electron microscopy (SEM) and EDS analysis by utilizing an SEM (JSM-76710F, JEOL, Tokyo, Japan), a transmission electron microscopy (TEM) (JEM-4010, JEOL, Tokyo, Japan), and a high-resolution TEM (HRTEM) (JSM-76710F, JEOL, Tokyo, Japan) operated at 300 kV accelerating voltage. X-ray photoelectron spectroscopy (XPS), Diffuse Reflectance Spectroscopy (DRS, SolidSpec-3700, Tokyo, Japan), and Raman spectroscopy (RAMAN, LabRAM HR-800, Chiba, Japan) analyses were performed by utilizing WI Tec. alpha 300 series. Porous characterization of $ZrO_2$-Ag-G and $ZrO_2$-Ag-G-$SiO_2$ structures was performed by a full analysis of $N_2$ adsorption/desorption tests (BELSORP-max, BEL Japan Inc., Tokyo, Japan). (PG201, Potentiostat, Galvanostat, Volta lab $^{TM}$, Radiometer, Aalborg, Denmark).

### 2.8. Electrochemical Measurements

Cyclic voltammetry (CV) and estimations were performed a three-electrode electrochemical set up to check the current and voltage profiles, where $ZrO_2$-Ag, $ZrO_2$-Ag-G, $ZrO_2$-Ag-G-$SiO_2$ was utilized as working electrode whereas platinum and Ag/AgCl electrode as counter and reference anodes, individually. Electrochemical properties in commercial urine were utilized with the measured pH 6.0, 6.7, and 6.5, individually. As electrolytes, 0.1 M NaOH, 0.1 M KOH, and Buffer were utilized. The following equation is used to determine the *LOD* [39–41]

$$LOD = 3\ SD/N \quad (1)$$

where *SD* is the standard deviation of the analyte concentration calculated from the current reaction of progressive including of glucose into the electrolyte; *N* is the slope of the calibration curve which demonstrates the affectability of the anode with a signal-to-noise ratio 3. Moreover, CV tests were performed from −0.3 to +0.2 V versus Ag/AgCl at a filter rate of 10 mV $s^{-1}$. All estimations were carried out by voltammetry (PG201, Potentiostat, Galvanostat, Volta lab $^{TM}$, Radiometer, Aalborg, Denmark).

## 3. Results

### *3.1. Characterization of the $ZrO_2$-Ag-G-$SiO_2$ Sample*

The mesoporous semiconductors were anchored on graphene nanosheets since this mesoporous conductive arrangement facilitates electron transport among nanostructure and electrolytes, hence making this a desirable stage for the design of biosensors. Figure 1 illustrates the crystalline characteristic properties of $ZrO_2$-Ag, $ZrO_2$-Ag-G, and $ZrO_2$-Ag-G-$SiO_2$ samples affirmed by the X-ray diffraction (XRD) technique.

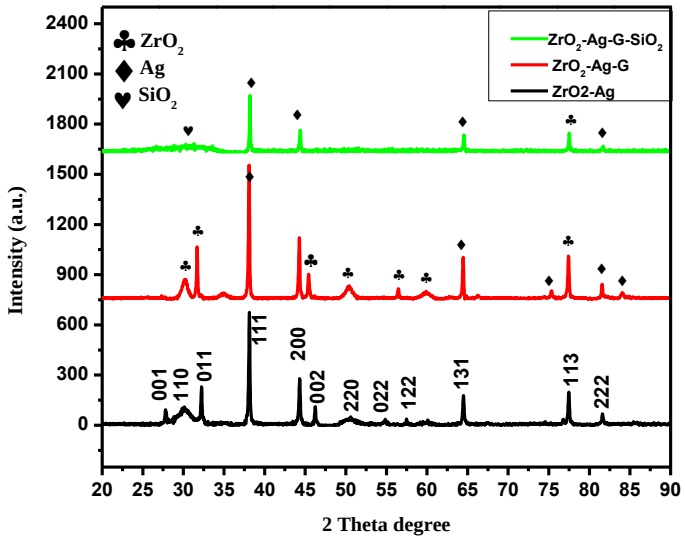


**Figure 1.** XRD patterns of $ZrO_2$-Ag, $ZrO_2$-Ag-G and $ZrO_2$-Ag-G-$SiO_2$.

The XRD patterns of the nanoparticles give the major 2y peak values at 25.6, 30.2, 32.9, 38.5, 44.6, 46.2, 50.2, 54.5, 55.2, 63.8, 76.4, and 84.5 in accordance with monoclinic zirconia. All diffraction peak values matched with the international standard file (JCPDS 37-1484). After modification, Ag nanoparticles could be indexed based on pure silver oxide having the symmetry of face center cubic. The peaks designated to the planes with the hkl values of 38.5 (111), 63.8 (131), 74.39 (220), and 80.58 (311), respectively, are the same with the XRD pattern of the (JCPDS 65-2871). After modification with $SiO_2$ the $ZrO_2$-Ag-G-$SiO_2$ all diffraction peaks along the (JCPDS 39-1425), affirming the crystalline nature of the samples.

The particle composition was also studied by TEM and SEM and the images are shown in Figure 2a–d.

Figure 2a showed the morphology of profoundly amplified TEM image of $ZrO_2$ which distributed as clustered in a flower shape. Morphology of $ZrO_2$ was also confirmed by SEM image (Inset). Figure 2b showed the TEM image of $ZrO_2$-Ag where Ag nanoparticles interconnected with $ZrO_2$. Figure 2c revealed the good distribution of $ZrO_2$-Ag on the Graphene surface. Figure 2d showed that the ZrO2-Ag G combined with mesoporous $SiO_2$. These figures showed that $ZrO_2$-Ag-G-$SiO_2$ were uniformly distributed. Every single TEM image is carried with a corresponding SEM image (Inset). Such flake-like nanostructured geometry leads to a rough surface of the electrode which can expectedly lead to an upgrade of the electrode performance on account of its high surface area, high surface-to-volume ratio, and exposure of more active sites on $ZrO_2$-Ag-G-$SiO_2$. Figure 2e,f showed the HRTEM image, the lattice space of 0.28 nm was given out to the interplanar of the (111) plane of the $ZrO_2$-Ag-G-$SiO_2$ sample and another lattice space of 0.26 nm was arranged to the interplanar of the (022) plane of the $ZrO_2$-Ag-G-$SiO_2$ sample.

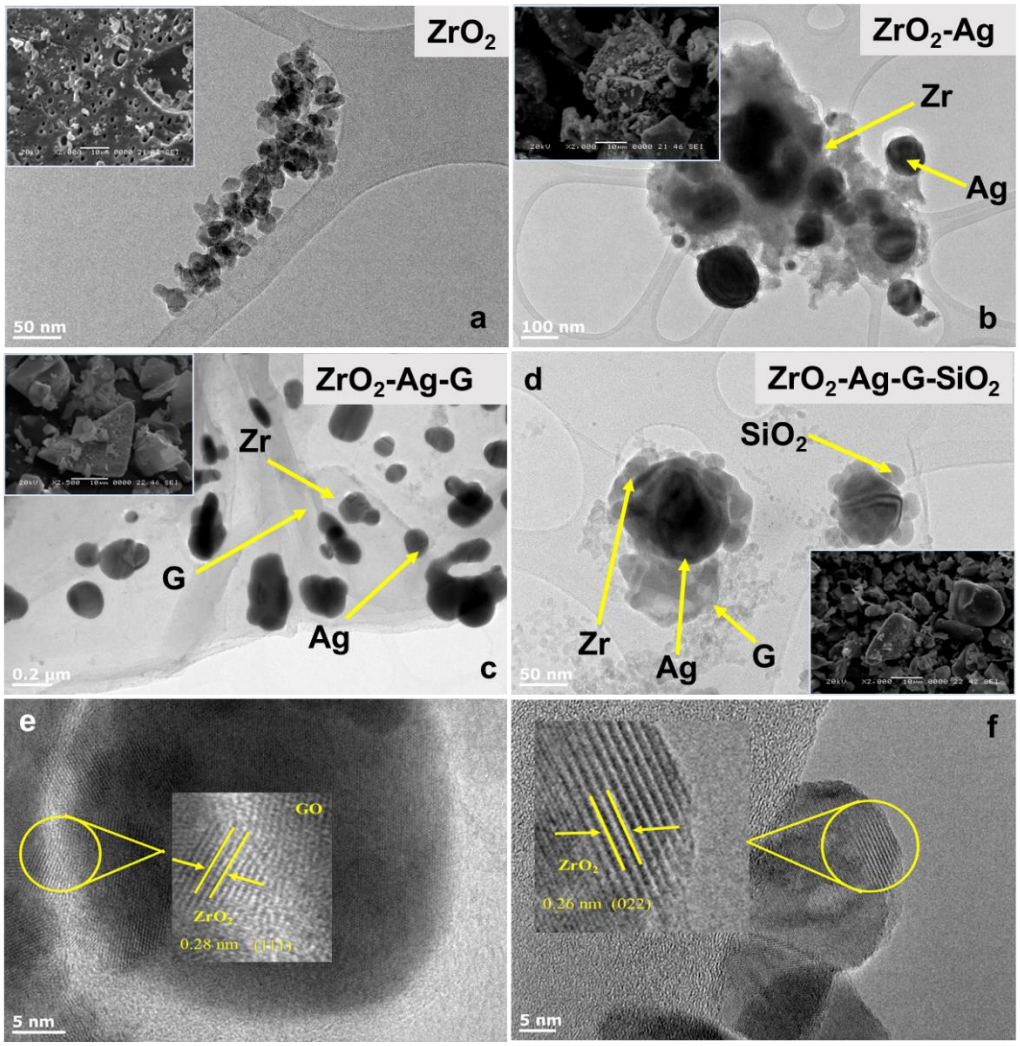


**Figure 2.** (**a**) $ZrO_2$ TEM Images and SEM Image (Inset), (**b**) $ZrO_2$-Ag TEM Images and SEM Image (Inset), (**c**) $ZrO_2$-Ag-G TEM Images and SEM Image (Inset), (**d**) $ZrO_2$-Ag G-$SiO_2$ TEM Images and SEM Image (Inset), and (**e**,**f**) HRTEM Images of $ZrO_2$ Ag-G-$SiO_2$.

The elemental state of the $ZrO_2$-Ag-G-$SiO_2$ nanoparticles was furthermore analyzed through EDS mapping.

As shown in Figure 3, the composition of $ZrO_2$-Ag-G-$SiO_2$ was presented to confirm the coexistence of Zr, C, Ag, and Si with the evaluated composition within the gravimetric rate of 29% Zr, 35% C, 12% Ag, and 5% Si.

Raman spectroscopy was also performed to characterize the G band showing in the composite.

As shown in Figure 4a, the G band of the as-synthesized sample appeared two peaks located at 1331 and 1573 $cm^{-1}$ corresponding to the (D band) and the C-C bond stretching frequency (G band), individually. For the most part, the intensity ratio of the D- and G bands (ID/IG) is utilized to evaluate the degree of disorder and the average size of $sp^2$ spaces. In this fact, the value of ID/IG was calculated to be 0.94.

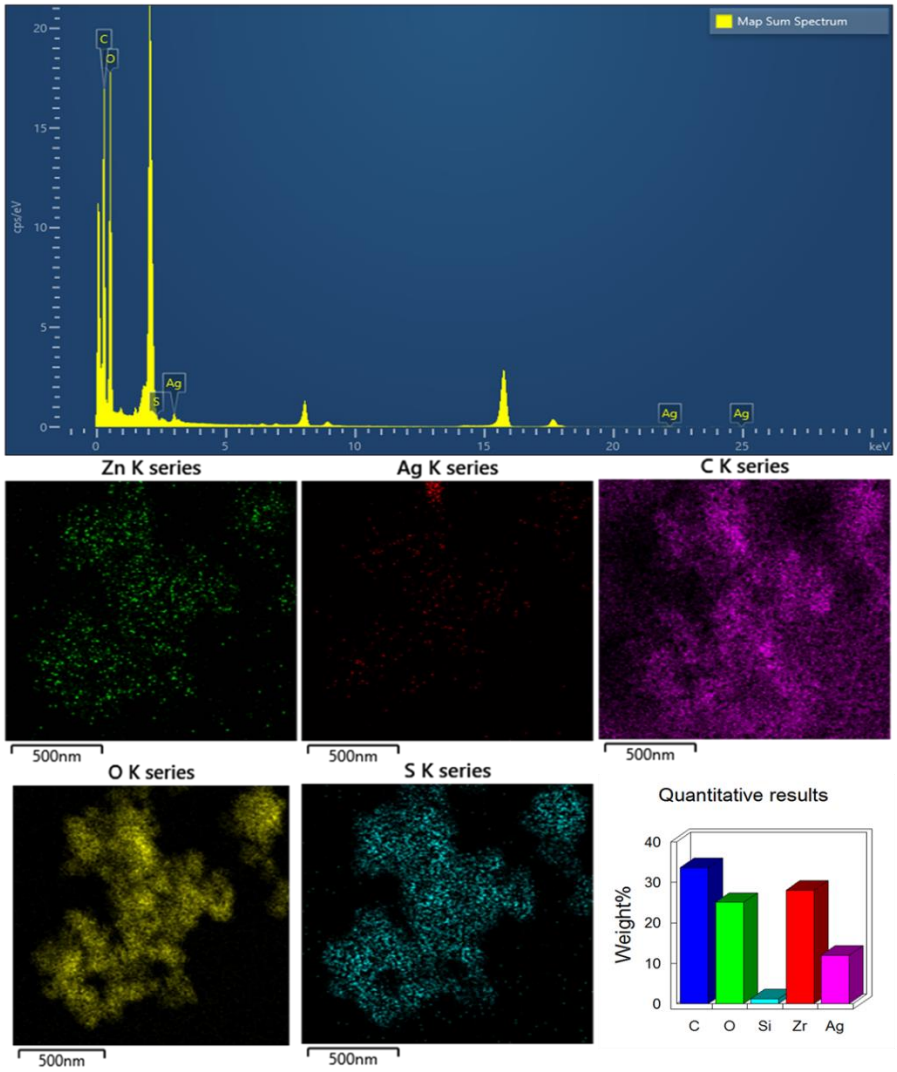


**Figure 3.** EDS mapping of $ZrO_2$-Ag-G-$SiO_2$ Samples.

The resultant absorbance of UV-DRS is depicted in Figure 4b. The optical bandgap of the $ZrO_2$-Ag, $ZrO_2$-Ag-G, $ZrO_2$-Ag-G-$SiO_2$, can be determined by the (Equation (2)): [42]

$$(\alpha hv)^{1/2} = A(hv - Eg) \quad (2)$$

where '$\alpha$' was the molar assimilation coefficient calculated as $\alpha = (1 - R)^2/2R$, $hv$ is the incident light frequency, '$A$' is the proportionality constant, and '$E_g$' is the bandgap energy of the material. Table 1 outlines the information form $(\alpha hv)^{1/2}$ as a function of photon energy. Band gaps showed 3.11 eV for Ag-doped $ZrO_2$-Ag and decrease after combining with graphene turned to 2.61 for the $ZrO_2$-Ag-G eV. Surprisingly, the band gaps change remarkably decreased to 2.00 eV within the $ZrO_2$-Ag-G-$SiO_2$ after combining through mesoporous $SiO_2$. Valence band (VB) and conduction band (CB) potentials of all the samples were calculated based on the following equations [43]

$$E_{CB} = X - Ee - \frac{1}{2} E_g \quad (3)$$

$$E_{VB} = E_{CB} + E_g \quad (4)$$

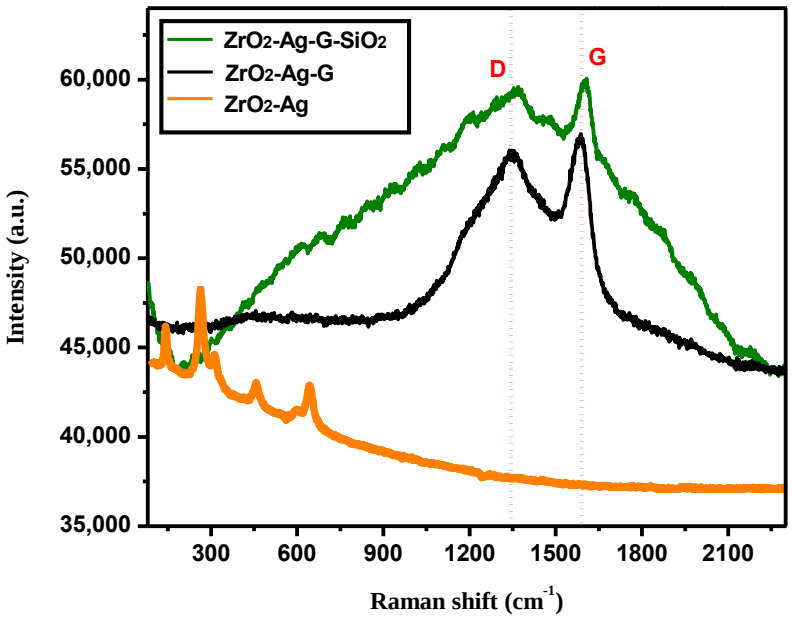


(**a**)

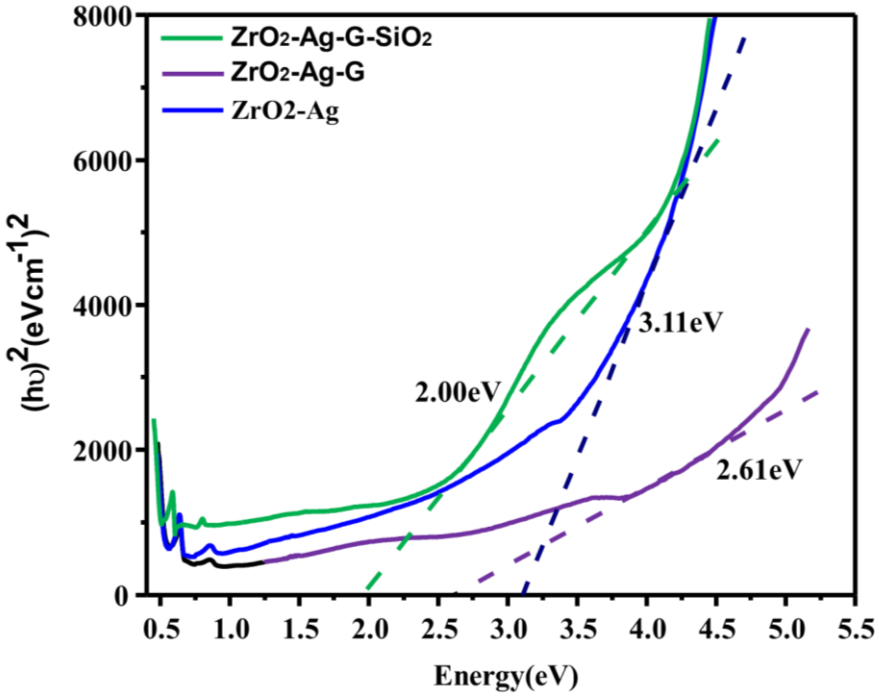


(**b**)

**Figure 4.** *Cont.*

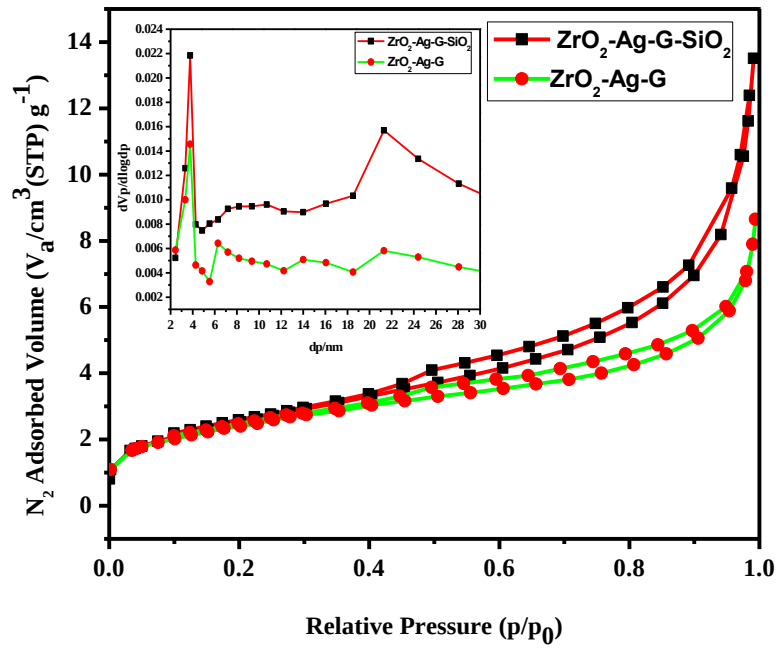


(**c**)

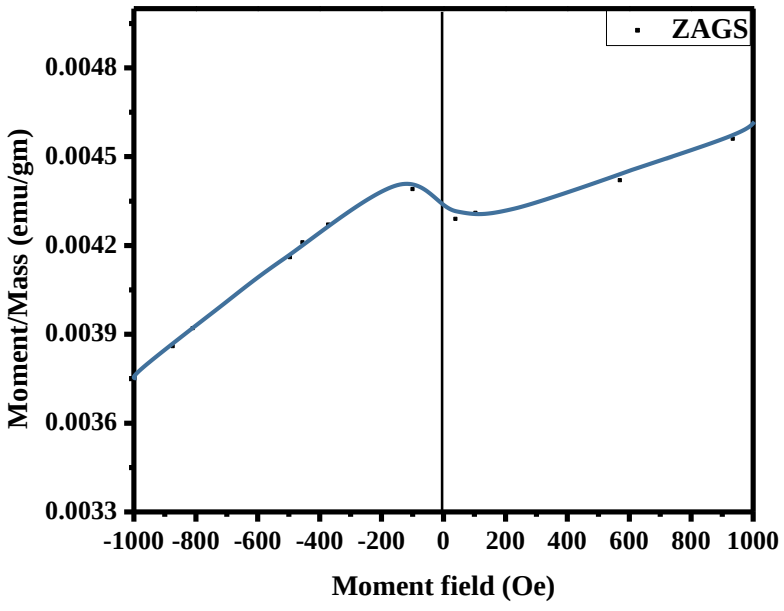


(**d**)

**Figure 4.** (**a**) Raman spectra of ZS, $ZrO_2$-Ag, $ZrO_2$-Ag-G, and $ZrO_2$-Ag-G-$SiO_2$ sample, (**b**) Nitrogen adsorption-desorption isotherms of $ZrO_2$-Ag-G, $ZrO_2$-Ag-G-$SiO_2$; and the corresponding pore size distributions (inset), (**c**) DRS data of $ZrO_2$-Ag, $ZrO_2$-Ag-G, $ZrO_2$-Ag-G-$SiO_2$ and (**d**) Magnetic field area of $ZrO_2$-Ag-G-$SiO_2$.

Here, $E_{VB}$ and $E_{CB}$ are valence and conduction band edge potentials, individually. c is the electronegativity of the semiconductor, $E_e$ is the energy of free electrons on the hydrogen scale and $E_g$ is the bandgap energy of the semiconductor.

**Table 1.** Surface properties obtained from nitrogen adsorption-desorption isotherms of ZAGS.

| №. | | BET Plot | | Bandgap Energy (eV) |
|---|---|---|---|---|
| | | **$ZrO_2$-Ag-G-$SiO_2$** | **$ZrO_2$-Ag-G** | |
| 1 | Total pore volume ($cm^3/g$) | 2.1069 [$cm^3$(STP) $g^{-1}$] | 1.9895 [$cm^3$(STP) $g^{-1}$] | $ZrO_2$-Ag-G 2.61 |
| 2 | Surface area ($m^2/g$) | 9.1703 [$m^2$ $g^{-1}$] | 8.6593 [$m^2$ $g^{-1}$] | ZrO2-Ag-G-$SiO_2$ 2.00 |
| 3 | Total pore volume ($p/p_0$ = 0.990) | 0.020549 [$cm^3$ $g^{-1}$] | 0.012273 [$cm^3$ $g^{-1}$] | |
| 4 | Mean pore diameter | 8.9632 nm | 5.6691 nm | |
| | | **BJH Plot** | | |
| | | **$ZrO_2$-Ag-G-$SiO_2$** | **$ZrO_2$-Ag-G** | |
| 1 | Mesopore surface area ($m^2/g$) | 8.064 [$m^2$ $g^{-1}$] | 5.8875 [$m^2$ $g^{-1}$] | |
| 2 | Mesopore volume ($cm^3/g$) | 0.01969 [$cm^3$ $g^{-1}$] | 0.011075 [$cm^3$ $g^{-1}$] | |
| 3 | Average mesopore diameter | 3.77 nm | 3.77 nm | |

Figure 4c presents the $N_2$ adsorption-desorption isotherms of $ZrO_2$-Ag-G and $ZrO_2$-Ag-G-$SiO_2$ samples. $ZrO_2$-Ag-G and $ZrO_2$-Ag-G-$SiO_2$ samples display typical type IV isotherm, illustrating those materials had mesopores. Isotherms of samples display an $H_2$ type hysteresis loop at a relative pressure ($P/P_0$) between 0.6 and 0.9, showing that these materials possess large and uniformly distributed mesopores. In addition, the hysteresis loops gradually shift to higher relative pressure ($P/P_0$) from $ZrO_2$-Ag-G to $ZrO_2$-Ag-G-$SiO_2$, proposing that these mesopores were extending with the counting mesoporous $SiO_2$. A mesopore diameter as large as 5.67 nm finds out the $ZrO_2$-Ag-G sample. When combining through mesoporous $SiO_2$ it proceeds to extend up to 8.96 nm as well as BET surface area also expanded from 8.66 to 9.17 $m^2$ $g^{-1}$, individually (Table 1). The electrochemical properties of nanocomposites were correlated with the BJH and BET analysis results. From BET analysis, the total pore volume and mean pore diameter of sensor active material are reduced due to the oxidizing agent treatment. According to the summary results of BET and BJH, the surface area and total pore mass of the graphene increased with $SiO_2$. The mesopore state and high surface area are the main parameters that are valuable for framing ion-transport tunnels in electrochemical reactions.

In magnetic field determination, one-level effective mass approximation (EMA) is utilized for a basic non-degenerate energy band. Bloch electrons in an energy band are treated as free electrons with the free electron mass m0 replaced by the effective mass m*. The Schrodinger equation for the function of the conduction electron in electric and magnetic fields can be shown with the following equation [43].

$$B = \frac{\mu 0 I}{2\pi r} \quad (5)$$

Figure 4d confirms the magnetic field curve of the $ZrO_2$-Ag-G-$SiO_2$ samples measured at ambient temperature. The saturation magnetization (MS), which is determined by the plot of M versus 1/H using data at low magnetic fields, is observed to be 0.0036.5 emu $g^{-1}$ to 0.0046.5 emu $g^{-1}$.

For characterizing detailed surface chemical compositions of $ZrO_2$-Ag-G-$SiO_2$, XPS analysis was performed.

The results are revealed in Figure 5. The complete spectrum of $ZrO_2$-Ag-G-$SiO_2$ shows the presence of Si, Zr, C, Ag, and O atoms attributed to the effective modification. The corresponding high-resolution spectra with respect to C1s signal 284.5 eV as a reference binding energy in Figure S1b attributed to C-C, bonds of graphene. As existing in Figure S1c, Si2P peaks were found at 102.8 eV. These peaks located at 184.08 eV correspond to Zr3d in Figure S1d. Besides, the interaction of the carbonyl group and hydroxyl group were also confirmed in O1s existing in Figure S1e with the binding energy at 531.6 eV corresponding to C-O bonds. Finally, the peaks at 367.0 eV and 373.1 eV revealed in Figure S1f correspond to Ag

3d. The overall results of the XPS study confirmed that all surface chemical compositions of $ZrO_2$-Ag-G-$SiO_2$ were found in the as-prepared nanocomposite.

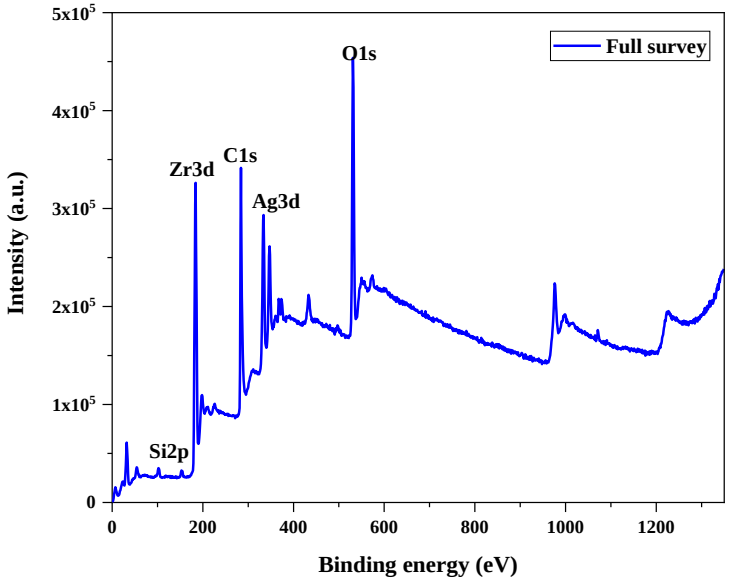


**Figure 5.** XPS spectra of $ZrO_2$-Ag-G-$SiO_2$ survey.

### *3.2. Electrocatalytic Activity of the $ZrO_2$-Ag-G-$SiO_2$ Electrode towards Glucose Sensing*

The electrochemical tests for working electrodes, $ZrO_2$-Ag, $ZrO_2$-Ag-G, $ZrO_2$-Ag-G-$SiO_2$ were performed in a three-electrode cell system with Pt wire as counter electrode and Ag/AgCl as a reference electrode within the potential range of −0.3 to +0.3 V. Figure 6a presents the CV profile of electrochemical responses in 10.5 mL of commercial urine and different electrolytes without glucose.

There was a poor oxidation peak observed in Figure 6a in the absence of glucose. In contrast, $ZrO_2$-Ag, $ZrO_2$-Ag-G, $ZrO_2$-Ag-G-$SiO_2$ electrodes showed a well-defined oxidation peak at the potential of +0.2 V. By adding 0.05 mmol/L of glucose, a poor response was noticed with the $ZrO_2$-Ag rather than $ZrO_2$-Ag-G and $ZrO_2$-Ag-G-$SiO_2$ electrode in the presence of glucose, due to the high bandgap energy of $ZrO_2$. After combining with Ag nanoparticle and graphene, the bandgap energy-reduced and $ZrO_2$-a supporting material for $ZrO_2$, rapidly transporting electrons during the electrochemical reaction due to their good conductive property. $ZrO_2$-Ag-G-$SiO_2$ electrode exhibited a substantial increase in anodic current density $4.0 \times 10^{-3}$ $mAcm^{-2}$ as showed in Figure 6b. For varying electrolytes such as 0.1 M phosphate buffer, NaOH, KOH, significant and fast current responses $9.0 \times 10^{-3}$ $mAcm^{-2}$ were observed for the $ZrO_2$-Ag-G-$SiO_2$ electrode with the addition of 0.55 mmol/L glucose as presented in Figure 6c. The obtained result clearly recommends the oxidation peak corresponds to the electro-oxidation of glucose at the $ZrO_2$-Ag-G-$SiO_2$ electrode [44]. Thus, a mechanism of non-enzymatic glucose sensing on the $ZrO_2$-Ag-G-$SiO_2$ electrode is clarified in Scheme 1.

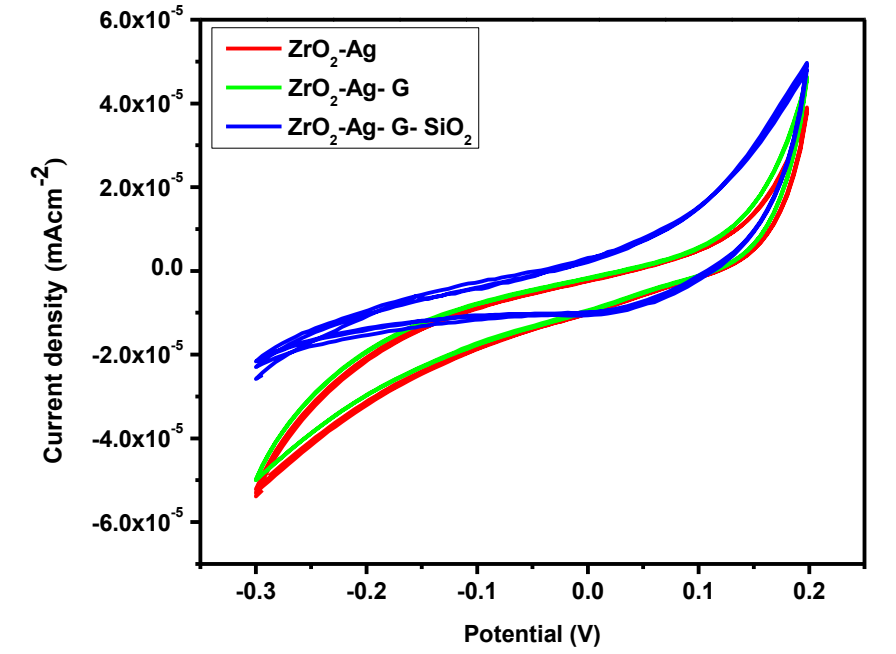


(**a**)

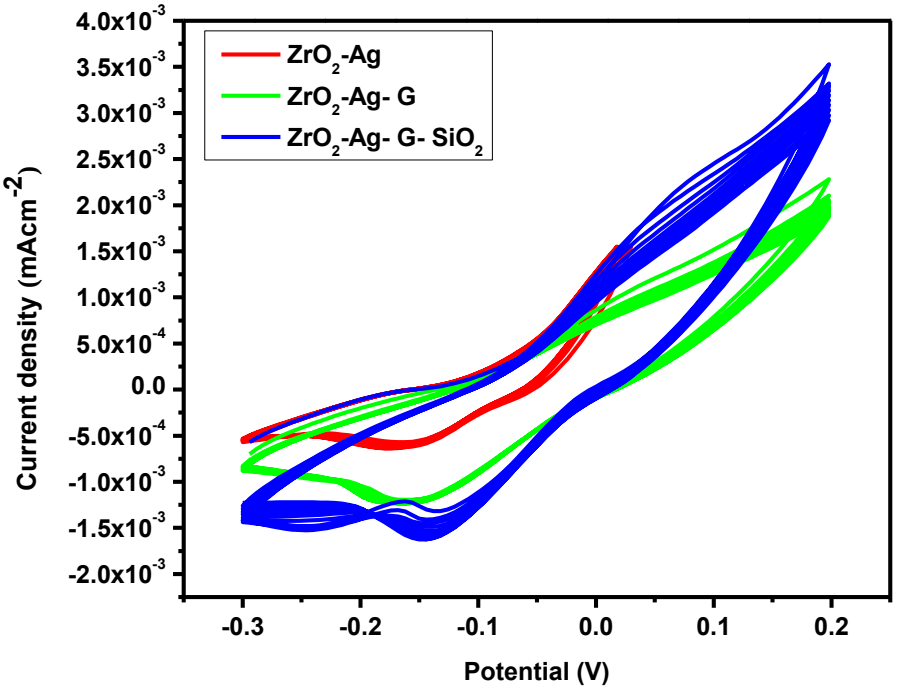


(**b**)

**Figure 6.** *Cont.*

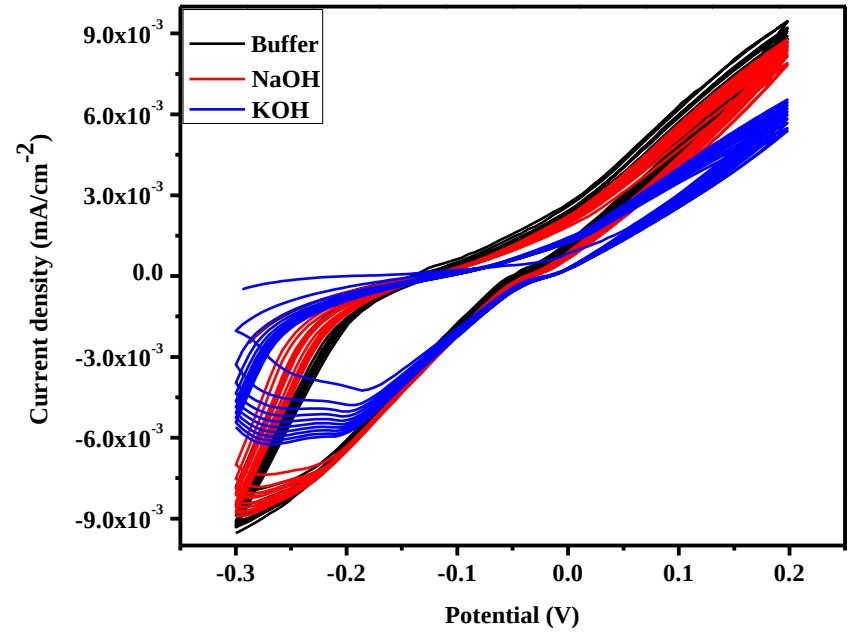


(**c**)

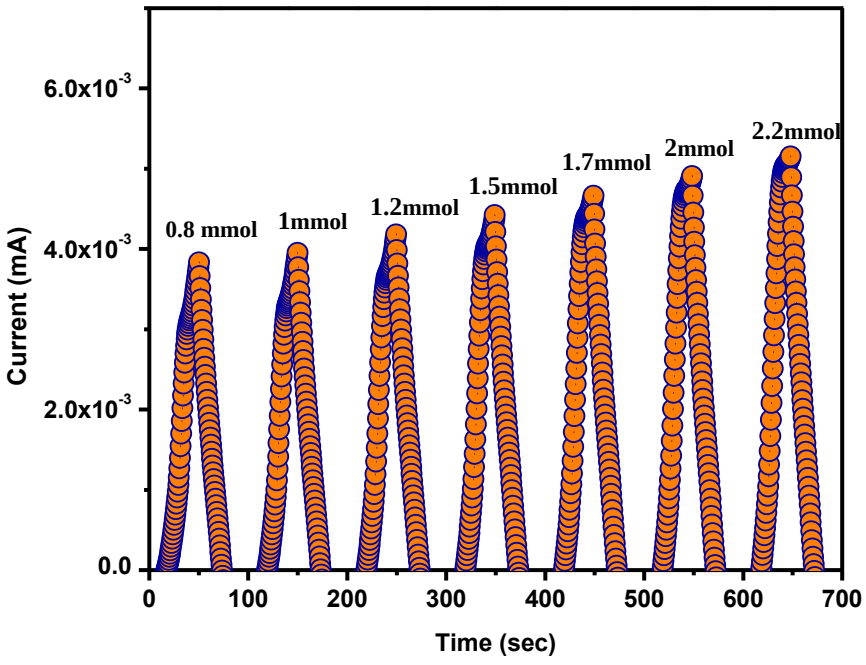


(**d**)

**Figure 6.** (**a**) Cyclic voltammogram of $ZrO_2$-Ag, $ZrO_2$-Ag-G, and $ZrO_2$-Ag-G-$SiO_2$ electrode in urine in the absence of glucose at a scan rate of 10 mV $s^{-1}$ (pH 7.0); (**b**) Cyclic voltammogram of $ZrO_2$-Ag, $ZrO_2$-Ag-G, and $ZrO_2$-Ag-G-$SiO_2$ sample with 0.05 mmol/L glucose in urine at a scan rate of 10 mV $s^{-1}$ (pH 7.0); (**c**) Cyclic voltammogram of $ZrO_2$-Ag-G-$SiO_2$ sample with different electrolyte: 0.1 M $PO_4^{3-}$Buffer (pH 7.4); 0.1 M NaOH (pH 13) and KOH (pH 13.5) at a scan rate of 10 mV $s^{-1}$ with the addition of 0.55 mmol/L glucose. (**d**) (i-t) curve of $ZrO_2$-Ag-G-$SiO_2$ sample with different conc. of glucose in 0.1 M PBS (pH 7.4). All experiments were run at room temperature (20 °C).

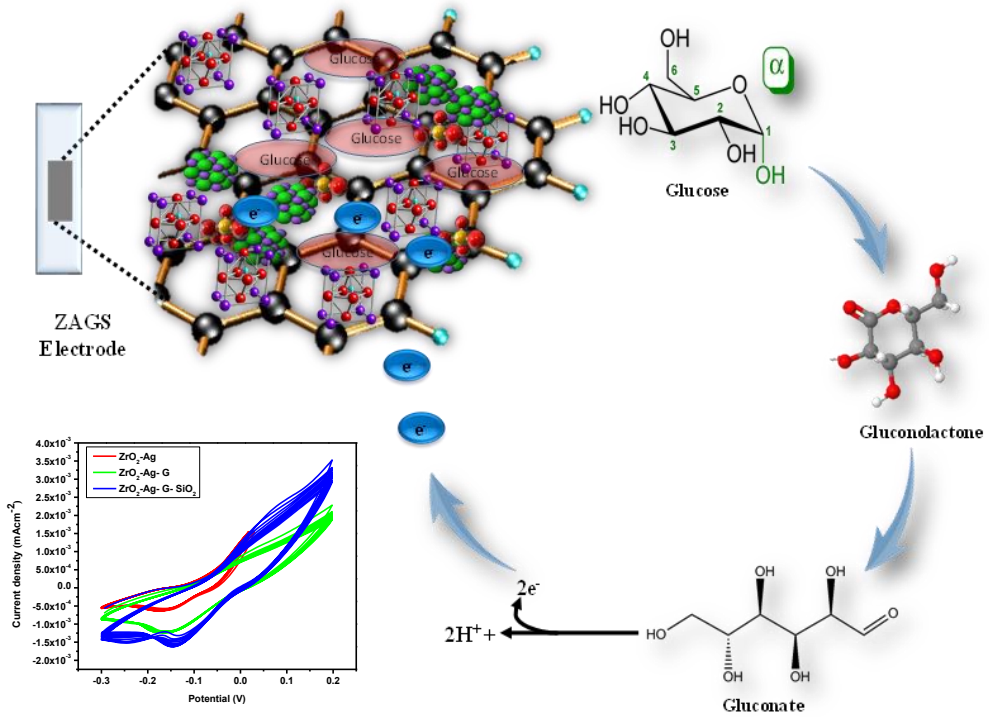


**Scheme 1.** The glucose-sensing mechanism of the ZAGS sample.

To demonstrate the analytical parameters (for example sensitivity, linear range, detection limit, and response time), the amperometric response of the $ZrO_2$-Ag-G-$SiO_2$ electrode was performed at a fixed voltage of +0.2 V (versus Ag/AgCl) in 0.1 M PBS by stepwise adding of glucose at different concentration. A well-defined and fast response to the $ZrO_2$-Ag-G-$SiO_2$ electrode was observed. Figure 6d confirms the current response which was estimated to be as high as $5.0 \times 10^{-3}$ mA $cm^{-2}$ at lower glucose concentration (0.05 mmol/L to 0.35 mmol/L). By adding glucose, the current response quickly reached a steady-state and attains ~98% of response within 1 s. The response current was linearly increased with increasing glucose concentration, $ZrO_2$-Ag-G-$SiO_2$ electrode exhibited high sensitivity in the linear range (0.05 mmol/L to 0.35 mmol/L).

Figure S4 displays the $ZrO_2$-Ag-G-$SiO_2$ glucose sensor calibration curve and cyclic voltammogram. With a linear range of 150–350 L and a correlation coefficient (R) of 0.996, the calibration curve indicated excellent linearity. Table S1 compares the detecting characteristics of several electrochemical glucose sensors, differentiating LOD and linear range. For glucose oxidation, the $ZrO_2$-Ag-G-$SiO_2$ sensor has a better linear response range and detection limit. The nanostructure of $ZrO_2$-Ag-G-$SiO_2$ offered greater surface area and exposed active sites, which facilitated electrolyte transport from solution to all active sites [45–49].

Overall, the enhanced sensing performance of the non-enzymatic glucose sensor is ascribed to the direct growth of mesoporous $ZrO_2$-Ag-G-$SiO_2$ thin film on FTO electrodes which offers a high surface area for $ZrO_2$ modification, resulting in fast electron transfer during the electrochemical process of glucose oxidation occurring between electrolyte and electrode. Importantly, we have used the self-assembly method to fabricate non-enzymatic $ZrO_2$-Ag-G-$SiO_2$ glucose-sensing electrodes which account for controllable nanostructures with great reproducibility and a cost-effective fabrication process for stable glucose sensing devices.

### *3.3. Selection of Electrolytes towards $ZrO_2$-Ag-G-$SiO_2$ Electrode*

Sensing of glucose by $ZrO_2$-Ag-G-$SiO_2$ sample with different electrolytes (PBS, NaOH; KOH) and different concentrations was investigated under ambient conditions. Glucose

oxidation with these electrolytes was measured in 0.1 M NaOH, phosphate buffer, and KOH by subsequent addition of 0.55 mmol/L of glucose at regular intervals and observed the current responses after every injection.

Figure 7a shows that when 0.55 mmol/L of glucose adding to different concentrations of electrolytes resulted in almost the best current density towards the phosphate buffer electrolytes. The current state of the $ZrO_2$-Ag-G-$SiO_2$ electrode greatly depends on glucose concentration and electrolyte pH (i.e., the amount of $OH^-$), since $OH^-$ are required to neutralize the protons generated during the dehydrogenation stage of the reaction. Hence, a better outcome is confirmed towards phosphate buffer for the $ZrO_2$-Ag-G-$SiO_2$ electrode.

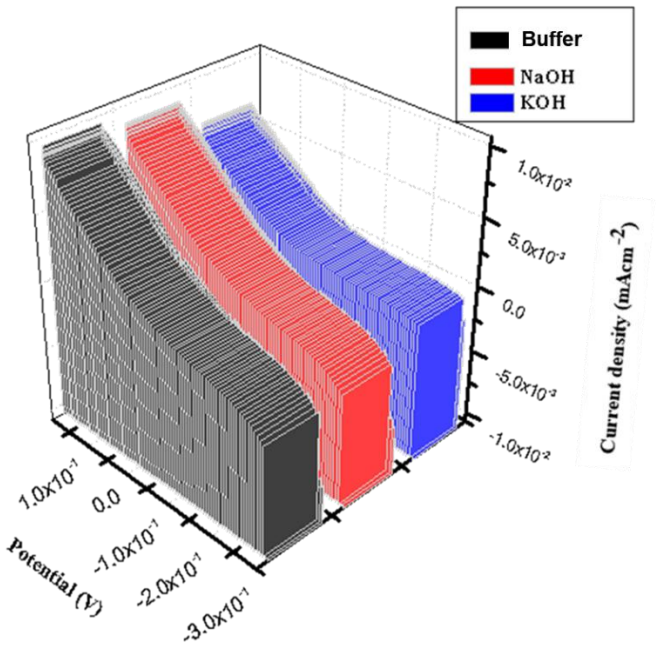


(**a**)

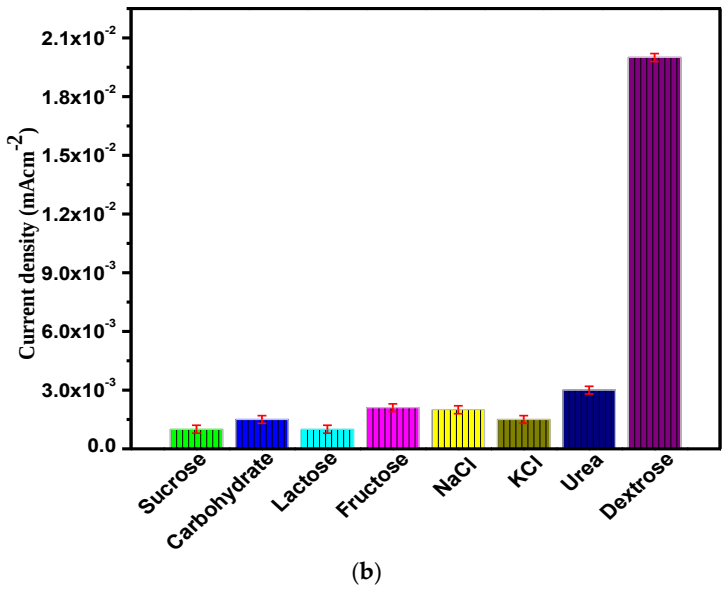


(**b**)

**Figure 7.** (**a**) Sensing of glucose by $ZrO_2$-Ag-G-$SiO_2$sample with different electrolytes: 0.1 M $PO_4^{3-}$ Buffer (pH 7.4); 0.1 M NaOH (pH 13) and KOH (pH 13.5) with the addition of 0.55 mmol/L glucose. (**b**) Selectivity test of glucose by the $ZrO_2$-Ag-G-$SiO_2$ sample with 0.91 mmol/L (Vitamin C, Starch, Lactose, Fructose, NaCl, KCl, Urea, and Glucose) in 0.1 M PBS (pH 7.4). All experiments were run at room temperature (20 °C).

As described above, the sensitivity and linear range of glucose sensing can be found by plotting peak current density against glucose concentrations as shown in Figure 7d. In 0.05 mmol/L glucose concentration, the sensor response had a sensitivity of $4.0 \times 10^{-3}$ mA $cm^{-2}$ and 0.35 mmol/L glucose concentration, the sensor response had a sensitivity of $5.0 \times 10^{-3}$ mA $cm^{-2}$. Here we can see that the response range is proportional to the concentration range. So, after observing this ratio we can easily reach this decision that we can measure a diabetic urine sample with this sensor for qualitative and quantitative analysis.

### *3.4. Anti-Interference Ability of the $ZrO_2$-Ag-G-$SiO_2$ Sensor*

The anti-interference ability of non-enzymatic-based glucose sensing devices is a major challenge, which could affect the electrode's sensing performance. To check the selectivity of $ZrO_2$-Ag-G-$SiO_2$ electrode in the presence of interfering species (such as Vitamin C, Starch, Lactose, Fructose, NaCl, KCl, and Urea), the amperometric response of the sensing electrode was checked by adding 0.91 mmol/L glucose and each above mentioned interfering species was in same concentration in the 0.1 M PBS solution at +0.2 V (versus Ag/AgCl), shown in Figure 7b. The addition of 0.91 mmol/L glucose leads to a rapid current response, although interfering species addition exhibited negligible current responses. As shown in the histogram of each interfering species addition and current response is shown here, which confirms the negligible current responses compared to 0.91 mmol/L glucose. These results suggest the suitability of the $ZrO_2$-Ag-G-$SiO_2$ electrode for the selective sensing of glucose in real samples. This confirmed that the $ZrO_2$-Ag-G-$SiO_2$ electrode was selective towards glucose without being affected by interferences. This enhanced sensing performance is basically attributed to a great interaction among the nanostructure and electrode with the high surface area for catalytic sites, facilitating a suitable path for electron transport during electrochemical activity. The results obtained with the proposed method were compared with other methods for the detection of glucose (Table S1). Overall, the $ZrO_2$-Ag-G-$SiO_2$ electrodes can be envisioned as a promising design for non-enzymatic glucose measurement in real clinical samples which may gain considerable benefits for different biomolecules sensing.

## 4. Discussion

The electrocatalytic properties of $ZrO_2$-Ag-G-$SiO_2$ were examined toward applications involving physiological pH, such as the detection of Glucose. Considering that glucose can be oxidized to gluconolactone (Scheme 1) at a neutral pH via a two-electron electrochemical reaction [50–52]. However, an excellent response was observed with the $ZrO_2$-Ag-G-$SiO_2$ sensor in the presence of glucose. This can be attributed to the excellent electrocatalytic nature of $ZrO_2$, which mediates the heterogeneous chemical oxidation or reduction of the glucose, while the converted $ZrO_2$ can be continuously and simultaneously recovered by electrochemical oxidation or reduction due to their high surface to volume ratio [51]. Additionally, in our sensor, the Ag-G-$SiO_2$ works as a supporting material for $ZrO_2$, rapidly transporting electrons during the electrochemical reaction due to their good conductive property. Also, the less dense morphology of the Ag-G-$SiO_2$ provides better permeability of the sensing matrix to the solution. The possible electrochemical reactions involved in glucose oxidation through the $Zr^{4+}/Zr^{3+}$ centers of $ZrO_2$ are given below [51]:

$$Zr^{4+} + \text{Glucose } (C_6H_{12}O_6) \rightarrow Zr^{3+} + \text{Gluconolactone } (C_6H_{10}O_6) + H_2O \quad (6)$$

$$\text{Gluconolactone } (C_6H_{10}O_6) + H_2O \rightarrow 2H^+ + \text{Gluconate } (C_6H_{12}O_7) \quad (7)$$

$$2Zr^{3+} \rightarrow 2Zr^{4+} + 2e^- \quad (8)$$

Therefore, electrooxidation of glucose on $ZrO_2$-Ag-G-$SiO_2$ for the nonenzymatic detection of glucose at physiological pH was investigated.

## 5. Conclusions

We developed a simple approach for producing $ZrO_2$-Ag-G-$SiO_2$ using the facile self-assembly method, producing a catalyst-coated and binder-free composite electrode. The $ZrO_2$-Ag-G-$SiO_2$ exhibited a uniform and highly mesoporous network of the catalytic film. Also, multiple active sites in $ZrO_2$-Ag-G-$SiO_2$ along with enhanced conductivity of graphene oxide improved the electrocatalytic performance of this electrode toward glucose oxidation. The ultra-high sensitivity ($9.0 \times 10^{-3}$ mA $cm^{-2}$) at a low applied potential of only 0.2 V versus Ag/AgCl, wide linear range (0.05 mmol/L–0.35 mmol/L), low sensing limit (0.05 mmol/L), with impressive qualitative and quantitative analysis, selectivity and stability make this $ZrO_2$-Ag-G-$SiO_2$ a promising electrode to serve as a non-enzymatic glucose sensor. Based on the results, $ZrO_2$-Ag-G-$SiO_2$ provided an excellent sensitivity in commercial urine specimens, so this biosensor is believed to have a high possibility for practical use.

**Supplementary Materials:** The following supporting information can be downloaded at: https://www.mdpi.com/article/10.3390/nano12020193/s1, Figure S1: XPs spectra of C1s (b), Si2p (c), Zr3d (d), O1s (e) and Ag3d (f); Figure S2: CV curve of $SiO_2$, Graphene, $ZrO_2$ and Ag; Figure S3: Pl data analysis of ZAGS; Table S1: Comparison of glucose detection method using various sensing electrodes.

**Author Contributions:** K.N.F.: Conceptualization, Formal Analysis, Investigation, Methodology, Validation, Visualization, writing—Original Draft, Review, and Editing. W.-C.O.: Conceptualization, Resources, Supervision, Writing Review, and Editing. C.-S.L.: Review and Editing. Y.L.: Review and Editing. K.-Y.C.: Review and Editing. C.-H.J.: Review and Editing. All authors have read and agreed to the published version of the manuscript.

**Funding:** This research received no external funding.

**Data Availability Statement:** Data are contained within the article.

**Conflicts of Interest:** The authors declare no conflict of interest.

## References

1. Mousavi, S.M.; Hashemi, S.A.; Gholami, A.; Mazraedoost, S.; Chiang, W.H.; Arjmand, O.; Omidifar, N.; Babapoor, A. Precise blood glucose sensing by nitrogen-doped graphene quantum dots for tight control of diabetes. *J. Sens.* **2021**, *2021*, 5580203. [CrossRef]
2. Tang, J.; Wei, L.; He, S.; Li, J.; Nan, D.; Ma, L.; Shen, W.; Kang, F.; Lv, R.; Huang, Z. A highly sensitive electrochemical glucose sensor based on room temperature exfoliated graphite-derived film decorated with dendritic copper. *Materials* **2021**, *14*, 5067. [CrossRef]
3. Xu, M.; Zhu, Y.; Gao, S.; Zhang, Z.; Gu, Y.; Liu, X. Reduced graphene oxide-coated silica nanospheres as flexible enzymatic biosensors for detection of glucose in sweat. *ACS Appl. Nano Mater.* **2021**, *4*, 12442–12452. [CrossRef]
4. Chen, H.C.; Su, W.R.; Yeh, Y.C. Functional channel of SWCNTs/$Cu_2O$/ZnO NRs/graphene hybrid electrodes for highly sensitive nonenzymatic glucose sensors. *ACS Appl. Mater. Interfaces* **2020**, *12*, 32905–32914. [CrossRef]
5. Fatema, K.N.; Liu, Y.; Cho, K.Y.; Oh, W.C. Comparative study of electrochemical biosensors based on highly efficient mesoporous $ZrO_2$-Ag-G-$SiO_2$ and $In_2O_3$-G-$SiO_2$ for rapid recognition of *E. coli* O157: H7. *ACS Omega* **2020**, *5*, 22719–22730. [CrossRef]
6. Fatema, K.N.; Zhu, L.; Cho, K.Y.; Jung, C.H.; Ullah, K.; Oh, W.C. Non-enzymatic sensing of glucose with high specificity and sensitivity based on high surface area mesoporous BiZnSbV-G-$SiO_2$. *J. Mater. Sci. Mater. Electron.* **2021**, *32*, 8330–8346. [CrossRef]
7. Fatema, K.N.; Oh, W.C. A comparative electrochemical study of non-enzymatic glucose, ascorbic acid, and albumin detection by using a ternary mesoporous metal oxide ($ZrO_2$, $SiO_2$ and $In_2$ $O_3$) modified graphene composite based biosensor. *RSC Adv.* **2021**, *11*, 4256–4269. [CrossRef]
8. Fatema, K.N.; Lim, C.S.; Oh, W.C. High surface area mesoporous BiZnSbV-G-$SiO_2$-based electrochemical biosensor for quantitative and rapid detection of microalbuminuria. *J. Appl. Electrochem.* **2021**, *51*, 1–16. [CrossRef]
9. Tripathi, K.M.; Ahn, H.T.; Chung, M.; Le, X.A.; Saini, D.; Bhati, A.; Sonkar, S.K.; Kim, M.I.; Kim, T. N, S, and P-Co-doped carbon quantum dots: Intrinsic peroxidase activity in a wide pH range and its antibacterial applications. *ACS Biomater. Sci. Eng.* **2020**, *6*, 5527–5537. [CrossRef] [PubMed]
10. Fatema, K.N.; Biswas, M.R.; Bang, S.H.; Cho, K.Y.; Oh, W.C. Electroanalytical characteristic of a novel biosensor designed with graphene–polymer-based quaternary and mesoporous nanomaterials. *Bull. Mater. Sci.* **2020**, *43*, 1–3. [CrossRef]
11. Fatema, K.N.; Sagadevan, S.; Liu, Y.; Cho, K.Y.; Jung, C.H.; Oh, W.C. New design of mesoporous $SiO_2$ combined $In_2O_3$-graphene semiconductor nanocomposite for highly effective and selective gas detection. *J. Mater. Sci.* **2020**, *55*, 13085–13101. [CrossRef]

12. Tripathi, K.M.; Bhati, A.; Singh, A.; Gupta, N.R.; Verma, S.; Sarkar, S.; Sonkar, S.K. From the traditional way of pyrolysis to tunable photoluminescent water soluble carbon nano-onions for cell imaging and selective sensing of glucose. *RSC Adv.* **2016**, *6*, 37319–37329. [CrossRef]
13. Li, X.; Liu, J.; Ji, X.; Jiang, J.; Ding, R.; Hu, Y.; Hu, A.; Huang, X. Ni/Al layered double hydroxide nanosheet film grown directly on Ti substrate and its application for a nonenzymatic glucose sensor. *Sens. Actuators B Chem.* **2010**, *147*, 241–247. [CrossRef]
14. Shu, Y.; Yan, Y.; Chen, J.; Xu, Q.; Pang, H.; Hu, X. Ni and NiO nanoparticles decorated metal–organic framework nanosheets: Facile synthesis and high-performance nonenzymatic glucose detection in human serum. *ACS Appl. Mater. Interfaces.* **2017**, *9*, 22342–22349. [CrossRef]
15. Farid, M.M.; Goudini, L.; Piri, F.; Zamani, A.; Saadati, F. Molecular imprinting method for fabricating novel glucose sensor: Polyvinyl acetate electrode reinforced by $MnO_2$/CuO loaded on graphene oxide nanoparticles. *Food Chem.* **2016**, *194*, 61–67. [CrossRef]
16. Yang, S.; Liu, L.; Wang, G.; Li, G.; Deng, D.; Qu, L. One-pot synthesis of $Mn_3O_4$ nanoparticles decorated with nitrogen-doped reduced graphene oxide for sensitive nonenzymatic glucose sensing. *J. Electroanal. Chem.* **2015**, *755*, 15–21. [CrossRef]
17. Balamurugan, J.; Thanh, T.D.; Karthikeyan, G.; Kim, N.H.; Lee, J.H. A novel hierarchical 3D N-Co-CNT@ NG nanocomposite electrode for non-enzymatic glucose and hydrogen peroxide sensing applications. *Biosens. Bioelectron.* **2017**, *89*, 970–977. [CrossRef]
18. Chung, J.S.; Hur, S.H. A highly sensitive enzyme-free glucose sensor based on Co3O4 nanoflowers and 3D graphene oxide hydrogel fabricated via hydrothermal synthesis. *Sens. Actuators B Chem.* **2016**, *223*, 76–82.
19. Naikoo, G.A.; Salim, H.; Hassan, I.U.; Awan, T.; Arshad, F.; Pedram, M.Z.; Ahmed, W.; Qurashi, A. Recent advances in non-enzymatic glucose sensors based on metal and metal oxide nanostructures for diabetes management—A review. *Front. Chem.* **2021**, *9*, 786. [CrossRef]
20. Cao, X.; Wang, N. A novel non-enzymatic glucose sensor modified with $Fe_2O_3$ nanowire arrays. *Analyst* **2011**, *136*, 4241–4246. [CrossRef]
21. Xia, C.; Ning, W. A novel non-enzymatic electrochemical glucose sensor modified with FeOOH nanowire. *Electrochem. Commun.* **2010**, *12*, 1581–1584. [CrossRef]
22. Pan, M.; Yin, Z.; Liu, K.; Du, X.; Liu, H.; Wang, S. Carbon-based nanomaterials in sensors for food safety. *Nanomaterials* **2019**, *9*, 1330. [CrossRef]
23. Ambrosi, A.; Chua, C.K.; Bonanni, A.; Pumera, M. Electrochemistry of graphene and related materials. *Chem. Rev.* **2014**, *114*, 7150–7188. [CrossRef] [PubMed]
24. Viswanathan, S.; Narayanan, T.N.; Aran, K.; Fink, K.D.; Paredes, J.; Ajayan, P.M.; Filipek, S.; Miszta, P.; Tekin, H.C.; Inci, F.; et al. Graphene–protein field effect biosensors: Glucose sensing. *Mater. Today* **2015**, *18*, 513–522. [CrossRef]
25. Liu, J.; Meng, X.; Hu, Y.; Geng, D.; Banis, M.N.; Cai, M.; Li, R.; Sun, X. Controlled synthesis of zirconium oxide on graphene nanosheets by atomic layer deposition and its growth mechanism. *Carbon* **2013**, *52*, 74–82. [CrossRef]
26. Gong, J.; Miao, X.; Wan, H.; Song, D. Facile synthesis of zirconia nanoparticles-decorated graphene hybrid nanosheets for an enzymeless methyl parathion sensor. *Sens. Actuators B Chem.* **2012**, *162*, 341–347. [CrossRef]
27. Liao, L.; Bai, J.; Lin, Y.; Qu, Y.; Huang, Y.; Duan, X. High-Performance Top-Gated Graphene-Nanoribbon Transistors Using Zirconium Oxide Nanowires as High-Dielectric-Constant Gate Dielectrics. *J. Adv. Mater.* **2010**, *22*, 1941–1945. [CrossRef]
28. Du, D.; Liu, J.; Zhang, X.; Cui, X.; Lin, Y. One-step electrochemical deposition of a graphene-$ZrO_2$ nanocomposite: Preparation, characterization, and application for detection of organophosphorus agents. *J. Mater. Chem.* **2011**, *21*, 8032–8037. [CrossRef]
29. Cho, B.H.; Ko, W.B. Preparation of graphene-$ZrO_2$ nanocomposites by heat treatment and photocatalytic degradation of organic dyes. *J. Nanosci. Nanotechnol.* **2013**, *13*, 7625–7630. [CrossRef]
30. Cho, B.; Ko, W. Preparation of $ZrO_2$-C60 nanocomposites using heat treatment and photocatalytic degradation of organic dyes. *Asian J. Chem.* **2013**, *25*, 4577–4582. [CrossRef]
31. Lee, Y.L.; Kim, S.; Park, C.; Ihm, J.; Son, Y.W. Controlling half-metallicity of graphene nanoribbons by using a ferroelectric polymer. *Acs Nano* **2010**, *4*, 1345–1350. [CrossRef] [PubMed]
32. Sandeep, S.; Santhosh, A.S.; Swamy, N.K.; Suresh, G.S.; Melo, J.S.; Mallu, P. Biosynthesis of silver nanoparticles using Convolvulus pluricaulis leaf extract and assessment of their catalytic, electrocatalytic and phenol remediation properties. *Adv. Mater. Lett.* **2016**, *7*, 383–389. [CrossRef]
33. Rosenholm, J.M.; Meinander, A.; Peuhu, E.; Niemi, R.; Eriksson, J.E.; Sahlgren, C.; Lindén, M. Targeting of porous hybrid silica nanoparticles to cancer cells. *ACS Nano.* **2009**, *3*, 197–206. [CrossRef] [PubMed]
34. Trewyn, B.G.; Slowing, I.I.; Giri, S.; Chen, H.T.; Lin, V.S. Synthesis and functionalization of a mesoporous silica nanoparticle based on the sol–gel process and applications in controlled release. *Acc. Chem. Res.* **2007**, *40*, 846–853. [CrossRef]
35. Amin, B.G.; Masud, J.; Nath, M. A non-enzymatic glucose sensor based on a $CoNi_2$ $Se_4$/rGO nanocomposite with ultrahigh sensitivity at low working potential. *J. Mater. Chem. B* **2019**, *7*, 2338–2348. [CrossRef]
36. Saraf, M.; Natarajan, K.; Mobin, S.M. Non-enzymatic amperometric sensing of glucose by employing sucrose templated microspheres of copper oxide (CuO). *Dalton Trans.* **2016**, *45*, 5833–5840. [CrossRef]
37. Biswas, M.R.; Oh, W.C. Comparative study on gas sensing by a Schottky diode electrode prepared with graphene–semiconductor–polymer nanocomposites. *RSC Adv.* **2019**, *9*, 11484–11492. [CrossRef]

38. Kwon, G.H.; Kim, T.W.; Lee, H.I.; Cho, W.C.; Kim, H. Synthesis of $ZrO_2$ nanorods and their applicati.on as membrane materials. *J. Korean Ceram. Soc.* **2019**, *56*, 541–548. [CrossRef]
39. Deng, Z.; Long, H.; Wei, Q.; Yu, Z.; Zhou, B.; Wang, Y.; Zhang, L.; Li, S.; Ma, L.; Xie, Y.; et al. High-performance non-enzymatic glucose sensor based on nickel-microcrystalline graphite-boron doped diamond complex electrode. *Sens. Actuators B Chem.* **2017**, *242*, 825–834. [CrossRef]
40. Zhou, Y.; Zheng, H.; Chen, X.; Zhang, L.; Wang, K.; Guo, J.; Huang, Z.; Zhang, B.; Huang, W.; Jin, K.; et al. The *Schistosoma japonicum* genome reveals features of host-parasite interplay. *Nature* **2009**, *460*, 345.
41. Zhan, B.; Liu, C.; Chen, H.; Shi, H.; Wang, L.; Chen, P.; Huang, W.; Dong, X. Free-standing electrochemical electrode based on Ni (OH) 2/3D graphene foam for nonenzymatic glucose detection. *Nanoscale* **2014**, *6*, 7424–7429. [CrossRef] [PubMed]
42. Zawadzki, W. Semiconductor electrons in electric and magnetic fields. *Surf. Sci.* **1973**, *37*, 218–243. [CrossRef]
43. Fatema, K.N.; Jung, C.H.; Liu, Y.; Sagadevan, S.; Cho, K.Y.; Oh, W.C. New Design of Active Material Based on $YInWO_4$-G-$SiO_2$ for a Urea Sensor and High Performance for Nonenzymatic Electrical Sensitivity. *ACS Biomater. Sci. Eng.* **2020**, *6*, 6981–6994. [CrossRef] [PubMed]
44. Ahmad, R.; Tripathy, N.; Ahn, M.S.; Bhat, K.S.; Mahmoudi, T.; Wang, Y.; Yoo, J.Y.; Kwon, D.W.; Yang, H.Y.; Hahn, Y.B. Highly efficient non-enzymatic glucose sensor based on CuO modified vertically grown ZnO nanorods on electrode. *Sci. Rep.* **2017**, *7*, 5715. [CrossRef]
45. Sedighi, A.; Montazer, M.; Mazinani, S. Synthesis of wearable and flexible NiP0. *1-SnOx/PANI/CuO/cotton towards a non-enzymatic glucose sensor. Biosens. Bioelectron.* **2019**, *135*, 192–199.
46. Chen, Y.; Zhong, Q.; Wang, Y.; Yuan, C.; Qin, X.; Xu, Y. Colorimetric detection of hydrogen peroxide and glucose by exploiting the peroxidase-like activity of papain. *RSC Adv.* **2019**, *9*, 16566–16570. [CrossRef]
47. Wang, B.; Ju, P.; Zhang, D.; Han, X.; Zheng, L.; Yin, X.; Sun, C. Colorimetric detection of $H_2O_2$ using flower-like Fe 2 $(MoO_4)_3$ microparticles as a peroxidase mimic. *Microchim. Acta.* **2016**, *183*, 3025–3033. [CrossRef]
48. Ma, Q.; Nakazato, K. Low-temperature fabrication of ZnO nanorods/ferrocenyl–alkanethiol bilayer electrode and its application for enzymatic glucose detection. *Biosens. Bioelectron.* **2014**, *51*, 362–365. [CrossRef]
49. Luo, J.J.; Pan, S.W.; Yang, J.H.; Chang, T.L.; Lin, P.Y.; Wu, C.L.; Liu, W.F.; Huang, X.R.; Koshevoy, I.O.; Chou, P.T.; et al. Detecting glucose levels in blood plasma and artificial tear by Au (I) Complex on the carbopol polymer: A microfluidic paper-based method. *Polymers* **2018**, *10*, 1001. [CrossRef]
50. Tomanin, P.P.; Cherepanov, P.V.; Besford, Q.A.; Christofferson, A.J.; Amodio, A.; McConville, C.F.; Yarovsky, I.; Caruso, F.; Cavalieri, F. Cobalt phosphate nanostructures for non-enzymatic glucose sensing at physiological pH. *ACS Appl. Mater.* **2018**, *10*, 42786–42795. [CrossRef] [PubMed]
51. Ahmad, R.; Ahn, M.S.; Hahn, Y.B. Fabrication of a non-enzymatic glucose sensor field-effect transistor based on vertically oriented ZnO nanorods modified with $Fe_2O_3$. *Electrochem. Commun.* **2017**, *77*, 107–111. [CrossRef]
52. Zhou, Y.; Ni, X.; Ren, Z.; Ma, J.; Xu, J.; Chen, X. A flower-like NiO–$SnO_2$ nanocomposite and its non-enzymatic catalysis of glucose. *RSC Adv.* **2017**, *7*, 45177–45184. [CrossRef]